frontiers | Frontiers in Physics

TYPE Original Research
PUBLISHED 03 April 2023
DOI 10.3389/fphy.2023.1172989

OPEN ACCESS

EDITED BY
San-Dong Guo,
Xi'an University of Posts and Telecommunications, China

REVIEWED BY
Zhang Tian,
Sichuan Normal University, China
Jun Li,
Southwest University, China

*CORRESPONDENCE
Bing Lv,
lvbing@gznu.edu.cn

†These authors have contributed equally to this work and share first authorship

SPECIALTY SECTION
This article was submitted to Physical Chemistry and Chemical Physics, a section of the journal Frontiers in Physics

RECEIVED 24 February 2023
ACCEPTED 17 March 2023
PUBLISHED 03 April 2023

CITATION
Yin X, Zhou L, Wang Q, Liao Y and Lv B (2023), High thermoelectric performance of $TlInSe_3$ with ultra-low lattice thermal conductivity.
Front. Phys. 11:1172989.
doi: 10.3389/fphy.2023.1172989

High thermoelectric performance of $TlInSe_3$ with ultra-low lattice thermal conductivity

Xixi Yin[1,2†], Lang Zhou[1,2†], Qi Wang[1,2], Yangfang Liao[1,2] and Bing Lv[1,2*]

[1]School of Physics and Electronic Science, Guizhou Normal University, Guiyang, China, [2]Key Laboratory of Low Dimensional Condensed Matter Physics of Higher Educational Institution of Guizhou Province, Guizhou Normal University, Guiyang, China

Thermoelectric (TE) materials with an excellent thermoelectric figure of merit (*ZT*) provide an effective way to alleviate energy pressure and protect the environment. By applying the first-principles method, this paper makes a systematic study of the electronic and phonon transport properties of two-dimensional (2D) novel $TlInSe_3$ utilizing the Boltzmann transport theory (BTE). The calculation results reveal that 2D $TlInSe_3$ has an excellent power factor (0.81×10^{-2} W/mK^2) and ultra-low lattice thermal conductivity (0.46 W/mK) at 300 K. We find that the low phonon group velocity and strong anharmonicity are the main factors leading to the ultra-low lattice thermal conductivity of $TlInSe_3$. Meanwhile, by discussing the acoustic-optical scattering, we attribute low phonon group velocity and strong anharmonicity to the increase of scattering rates between acoustic mode and optical mode, which further suppresses the lattice thermal conductivity. In the analysis of electron and phonon transport properties, 2D $TlInSe_3$, as a novel TE material, exhibits a *ZT* value as high as 4.15 at 500 K. Our research results show that $TlInSe_3$ is a potential TE material, and the relevant analysis is significant in exploring new TE materials.

KEYWORDS

first-principles calculation, ultra-low lattice thermal conductivity, phonon anharmonicity, 2D $TlInSe_3$, high thermoelectric performance

1 Introduction

The thermoelectric effect enables the conversion of waste heat to electrical energy, while the conversion efficiency of thermoelectric (TE) materials can be evaluated by the thermoelectric figure of merit (*ZT*) value, demonstrated in the formula: $ZT = \frac{S^2\sigma T}{k_l + k_e}$, where S is the Seebeck coefficient; σ represents electrical conductivity,; k_l; k_e are lattice and electronic thermal conductivity, respectively [1]. In recent years, in order to increase the ZT value, researchers have employed phonon or electronic engineering techniques to reduce k_l or increase the power factor ($PF = S^2\sigma$) [2–4]. However, due to the mutual coupling between the TE parameters (S; σ; k_e) [5, 6], it achieved a negligible boost of ZT [7]. Therefore, a new material with intrinsic ultra-low k_l may offer exciting prospects to achieve higher ZT and thus realize its own potential utilization in TE fields.

Recent research has shown that thallium (Tl) compounds possess intrinsically ultra-low lattice thermal conductivity (k_l) [8–11]. For example, in Kurosaki's research, the binary and ternary thallium compounds demonstrated ultra-low k_l, in which the approximate value of k_l of $TlInTe_2$ is 0.5 W/mK at room temperature, almost one-third that of Bi_2Te_3 (~1.4 Wm/K) [8, 11, 12]. In addition, three-dimensional (3D) thallium selenide (TlSe) was synthesized

by Dutta, displaying its intrinsic ultra-low k_l of 0.62–0.4 W/mK [10]. However, the *ZT* of bulk Tl compounds (*ZT* value of $TlInTe_2$ is 1.78, Tl_9BiTe_6 is about 1, and Tl_4ZrTe_4 is only 0.16) is low compared to other TE materials because of the low power factor (*PF*) [7, 13–19]. Therefore, an ultra-low k_l and a high *PF* is necessary to obtain a high *ZT* value. Fortunately, two-dimensional (2D) materials can provide excellent *PF* values, especially 2D selenium compounds, such as Bi_2Se_3, Ag_2Se, SnSe, InSe, *etc.*, where the PF value of InSe is 0.049 W/mK^2 at 300 K, which is six times more than its bulk material [16, 20–24]. Moreover, experimentally synthesized Group III monolayer metal sulfides, such as In_2Se_3, GaSe, *etc.*, have been widely studied because of their distinctive TE properties [15, 20, 25, 26]. Considering that Tl is in the same group as Ga and In elements, and the high electronegativity and the lone pair electrons in Tl, it is feasible to design a new type of thallium chalcogenide semiconductor. Indeed, many ternary and binary thallium chalcogenides have been studied for their TE properties [9–11, 16, 27]. However, it is worth noting that previous investigations into Tl compounds were mainly laboratory work, while the inherent physical mechanism of the ultra-low k_l remains unclear. In addition, the ternary compounds formed by substituting the same group of elements have also attracted the attention of researchers due to their unique thermoelectric properties [28–32]. Therefore, inspired by these factors, it is urgent to design a novel 2D ternary compound material containing thallium, thallium congeners, and selenium elements to verify whether this can become a new and effective way to obtain materials with high thermoelectric performance.

This work employs the Boltzmann transport theory (BTE), taking $TlInSe_3$ as a typical example, to study its electron and phonon transport properties combined first principles. Our research shows that, at room temperature, $TlInSe_3$ has a *ZT* value of up to 4.15 at 500 K and an ultra-low k_l of 0.46 W/mK. In addition, we find that the lower phonon group velocity and the large phonon anharmonicity are the main factors leading to the extremely low k_l of $TlInSe_3$. Meanwhile, by discussing the phonon scattering channels, we find that the increase of the A + O/A→O ("A" is acoustic mode, "O" for optical mode) scattering channel leads to low phonon group velocity, which further suppresses the lattice thermal conductivity.

2 Computational and theoretical methods

We perform density functional theory (DFT) calculations using the QUANTUM ESPRESSO (QE) code [33, 34]. To obtain the relaxation structure and energy band structure, we use the kinetic energy of 70 Ry, the k-points of 16 × 16 × 1; and the energy convergence standard is 10^{-9} Ry, while the force convergence standard is 10^{-8} Ry. 16 × 16 × 1 k-points and 8 × 8×1 q-points are set to calculate phonon dispersion based on density functional perturbation theory (DFPT) [35, 36]. Meanwhile, based on periodic boundary conditions, in the 2D $TlInSe_3$ *z*-direction, we set a vacuum layer of 35 Å to prevent out-of-plane interactions. By working out the phonon Boltzmann transport equation, the k_l of 2D $TlInSe_3$ is obtained in the ShengBTE code [37]. A scaling parameter of 1.0 and a q-point grid of 60 × 60 × 1 are set. 3 × 3 × 1 supercell, together with a 4 × 4 × 1 k-mesh, is used to get the third-order interatomic force constants (IFCs). Supplementary Figure S1 shows the convergence of k_l with different cutoff radii of third-order, the k_l converges when the cutoff radius takes into account the 10th nearest neighbor. The electron transport properties considering electron-acoustic interactions are further studied by the PERTURBO software [38–41]. The maximum local Wannier function is built, through which the s, p orbitals of Tl atoms, the s, p orbitals of In atoms, and the p orbitals of Se atoms were selected by projecting the density of states.

In addition, to determine convergence, we tested the mobility using dense k-points, as demonstrated in Supplementary Figure S2A,B, which show that holes using 160 × 160 × 1 k-points and q-points can achieve convergence, while for electrons, it is necessary to use 480 × 480 × 1 k-points and a q point of 160 × 160 × 1 to ensure convergence.

In PERTURBO, $\tau_{nk} = \Gamma_{nk}^{-1}$ is employed to calculate the relaxation time, where Γ_{nk} is the scattering rate defined as

$$\Gamma_{nk} = \frac{1}{N_q}\sum_{m,vq} W_{nk,mk+q}^{vq}, \tag{1}$$

In the above equation, $W_{nk,mk+q}^{vq}$ is the scattering probability. The conductivity is computed as

$$\sigma_{\alpha\beta} = e^2 \int dE\left(-\frac{\partial f^0}{\partial E}\right)\sum_{\alpha\beta}(E), \tag{2}$$

where $\sum_{\alpha\beta}(E)$ is the transport distribution function at energy *E*, while *a* and *β* are Cartesian directions. The Seebeck coefficient (*S*) is computed from the $\sum_{\alpha\beta}(E)$ using the formula

$$S_{\alpha\beta} = \frac{e}{T}\int dE\left(-\partial f^0/\partial E\right)(E-\mu)\sum_{\alpha\beta}(E), \tag{3}$$

where μ is the chemical potential and T is the temperature. The electronic thermal conductivity is obtained by the formula

$$K_{\alpha\beta} = \frac{1}{T}\left\{\frac{\left(\int \sum_{\alpha\beta}(E)(E-\varepsilon_F)\left[-\frac{\partial f^0}{\partial E}\right]\right)^2 dE}{\int \sum_{\alpha\beta}(E)\left[-\frac{\partial f^0}{\partial E}\right]dE} - \int \sum_{\alpha\beta}(E)(E-\varepsilon_F)^2\left[-\frac{\partial f^0}{\partial E}\right]dE\right\}, \tag{4}$$

where ε_F is the Fermi level of a certain doping.

3 Results and discussions

The top and side drawings of the novel 2D $TlInSe_3$ are plotted in Figure 1A. The 2D $TlInSe_3$ is a hexagonal structure and is the P-3m1 space group. The optimized lattice constant is 4.17 Å, which is in agreement with the results in the literature [20, 42, 43]. Figure 1B shows the phonon spectrum of the novel 2D $TlInSe_3$. Since 2D $TlInSe_3$ has no imaginary frequency, its structure is dynamically stable. Meanwhile, we have tested the energy with different k-points, and compared the phonon dispersion by using the q points of 7 × 7 × 1 and 9 × 9 × 1, and found no difference, indicating that the phonon spectrum is convergent, as shown is Supplementary Figure S3A,B. At the same time, It is noteworthy that near the Γ point, the coupling exists between acoustic and optical phonons, suggesting that there is acoustic-optic scattering interaction. In addition, the

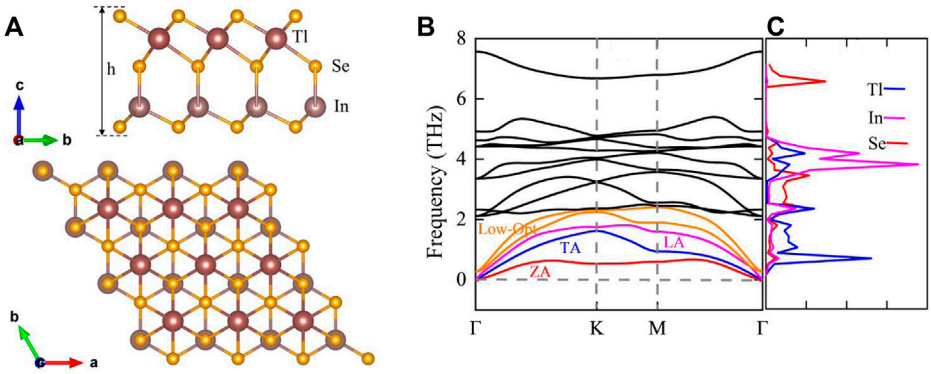

FIGURE 1
(A) Relaxed structure of 2D $TlInSe_3$, h is effective thickness, **(B)** phonon band plots where the red line represents the ZA mode, the blue line the TA mode, the magenta line the LA mode, the orange line the low-frequency optical mode, and the black line the high-frequency optical mode, and **(C)** DOS for 2D $TlInSe_3$.

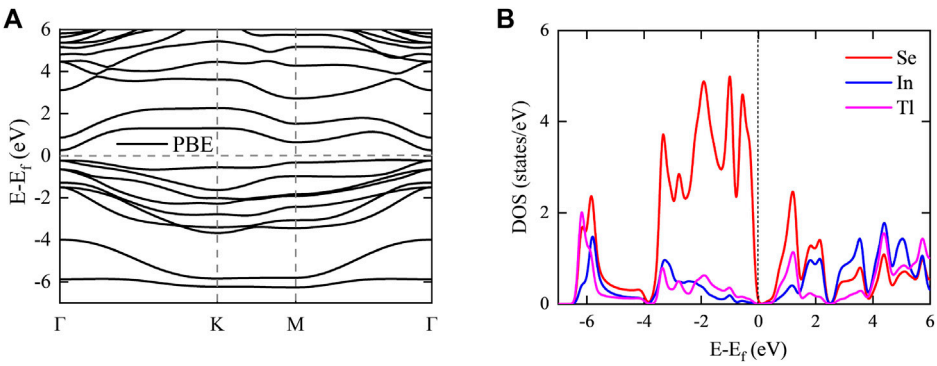

FIGURE 2
(A) The band structures without SOC, and **(B)** projected density of states of 2D $TlInSe_3$, respectively.

ZA and TA modes have an apparent concave, indicating the softening of acoustic phonons, which is beneficial to reduce the lattice thermal conductivity. In addition, the ZA mode is relatively smooth, suggesting that the ZA mode has a smaller phonon group velocity. The phonon density of states (DOS) of 2D $TlInSe_3$ is presented in Figure 1C. Since the atomic mass of thallium (Tl) is larger than that of In atoms and selenium (Se) atoms, it controls the acoustic branch and part of the low-frequency optical branch, while the optical branch is mostly dominated by the vibration of Indium (In) atoms.

Moreover, we study further the cohesive energy (E_{coh}) of $TlInSe_3$, whose formula is as follows:

$$E_{coh} = \frac{N_{Tl}E_{Tl} + N_{In}E_{In} + N_{Se}E_{Se} - E_{TlInSe3}}{N_{Tl} + N_{In} + N_{Se}}, \quad (1a)$$

Among them, N represents the number of atoms of each element, E is the energy of a single atom of each element, and $E_{TlInSe3}$ is the total energy of 2D $TlInSe_3$. The calculated E_{coh} is 0.32 eV, indicating that its structure is energetically favorable.

The *ab initio* molecular dynamics (AIMD) has been simulated using a 3 × 3 supercell at different temperatures with a time setting of 5 ps and a time step of 1 fs. Due to the small fluctuation in the total energy, the atomic structure exhibits only a small deviation from its equilibrium position at 300 and 500 K. These studies show that 2D $TlInSe_3$ is stable at 300 and 500 K. However, at 700 K, as shown in Supplementary Figure S4, there is significant distortion with large fluctuations in energy, and the $TlInSe_3$ monolayer is unstable.

Figure 2A shows the electronic energy bands of $TlInSe_3$ without considering the w-SOC (with the spin-orbit coupling). Meanwhile, it shows that the energy band structure of $TlInSe_3$ has a double degeneracy at the Γ point, which is beneficial for obtaining a high power factor. In Supplementary Figures S3A,B, the energy band structures considering the w-SOC and without considering the spin-orbit coupling are basically the same. Moreover, our study of the electronic band structure also reveals 2D $TlInSe_3$ as an indirect-band-gap material, which is also in line with previous studies [20, 43]. The projected density of states (DOS)in Figure 2B reveals that Se atoms are predominant near the valence band maximum (VBM), as

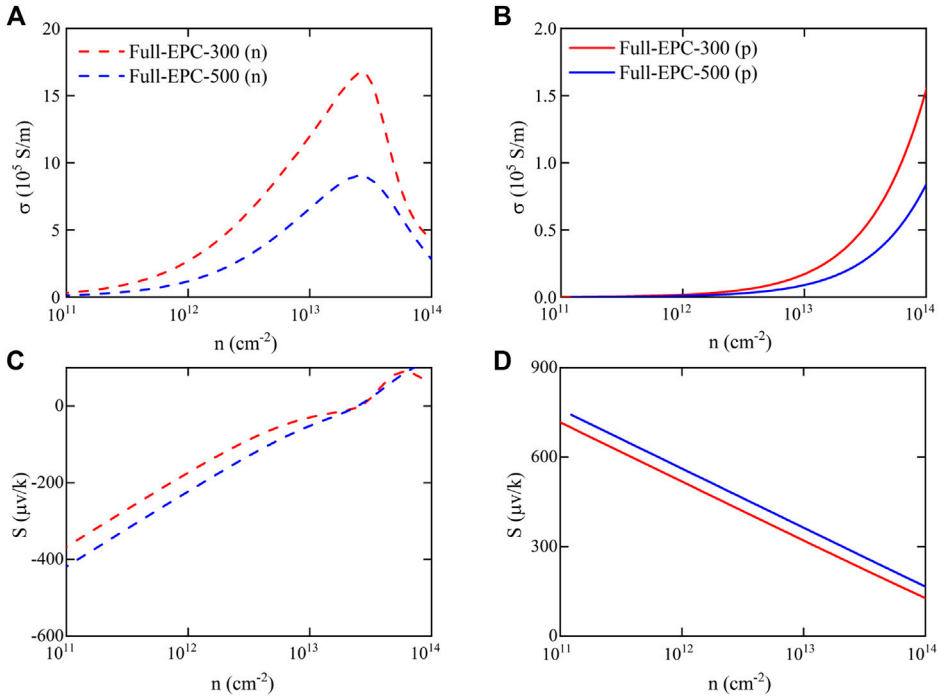

FIGURE 3
(A,B) Conductivity σ and **(C,D)** Seebeck coefficient S as a function of electrons and holes at 300, and 500 K, respectively.

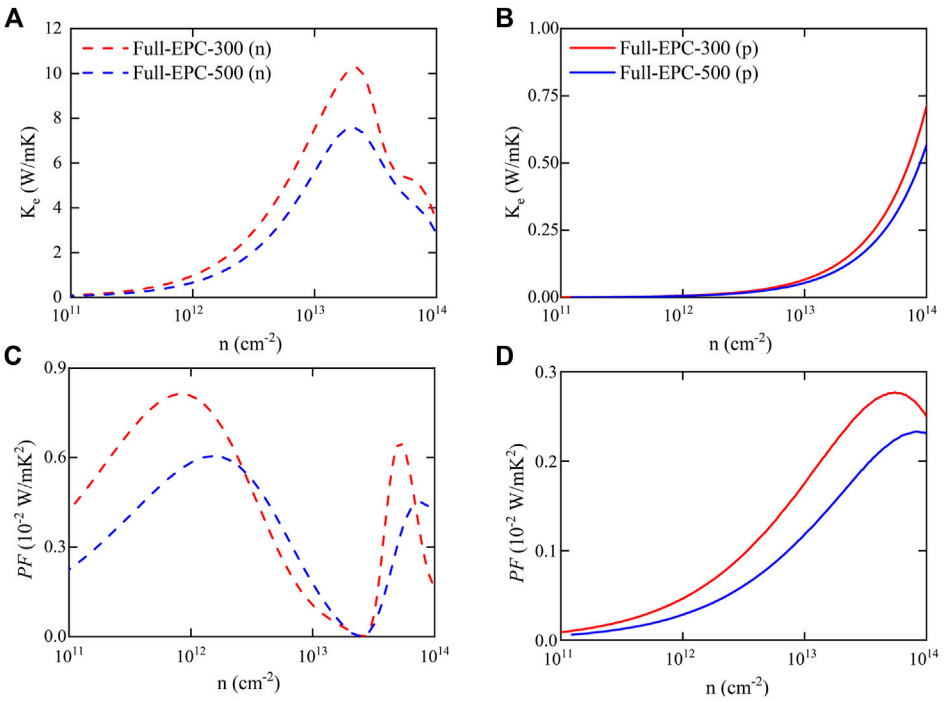

FIGURE 4
(A) and **(B)** are k_e, **(C)** and **(D)** are $S^2\sigma$ (PF) for 2D $TlInSe_3$ at 300 K and 500 K, respectively.

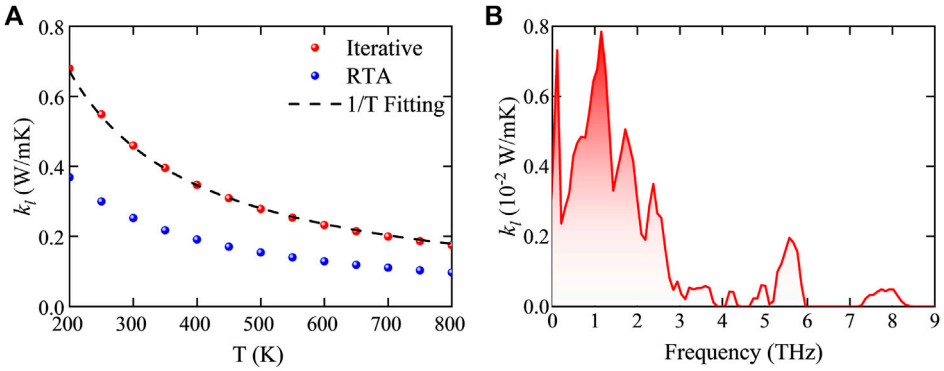

FIGURE 5
(A) The k_l of novel 2D $TlInSe_3$ at different temperatures. **(B)** Cumulative plot of k_l at different frequencies.

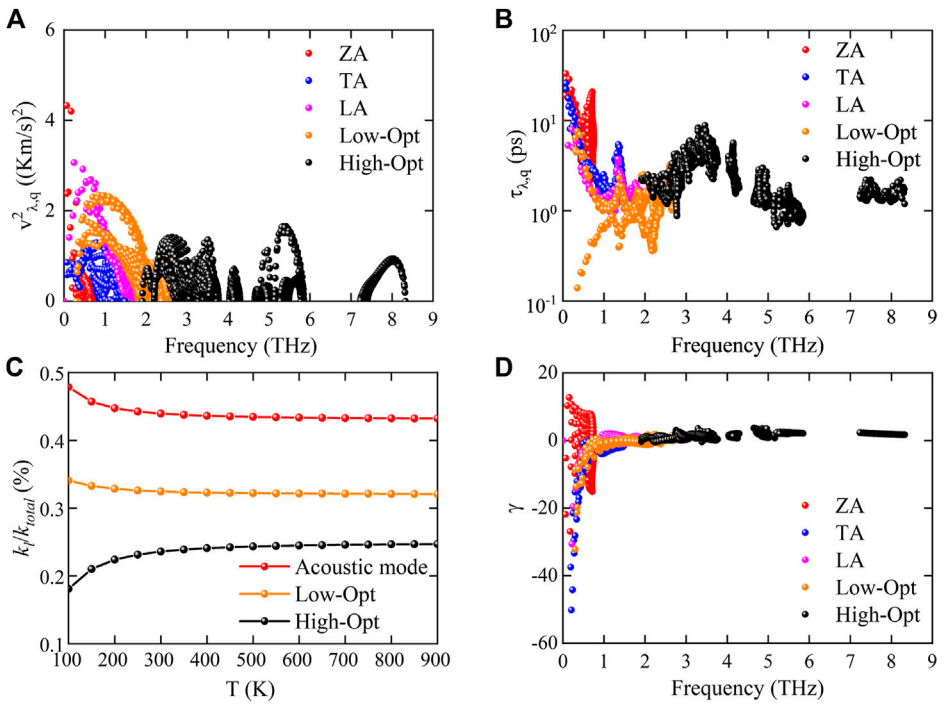

FIGURE 6
(A) The $v_{\lambda,q}$, **(B)** $\tau_{\lambda,q}$, **(C)** contribution of different phonon modes to the total k_l (percentage), **(D)** γ parameter of 2D $TlInSe_3$ at room temperature, respectively.

well as the conduction band minimum (CBM). Supplementary Figure S6 displays that the PBE band is in good agreement with those constructed by Wannier 90. Since performing QE and Perturbo software to calculate electron transport properties under electron-phonon interactions does not support HSE, therefore, we use the PBE function to carry out these calculations.

The electron transport coefficients of $TlInSe_3$ are obtained by solving the Boltzmann transport equation (BTE). The electron conductivity (σ) and the Seebeck coefficient (S) as a function of the carrier concentration from 300–500 K are demonstrated in Figures 3A–D. The calculation results clearly show that the σ of n-type doping is an order of magnitude, that is, higher than that of p-type doping, as presented in Figures 3A, B. For n-type doping, σ first arises and then goes down with carrier concentration because of the sudden drop in mobility at high concentrations when considering electron-phonon (el-ph) coupling, which was also reported in previous literature [44–47]. The $TlInSe_3$ monolayer shows a large S (absolute value) under n-type and p-type doping, as displayed in Figures 3C, D. Moreover, the S (absolute value) of 2D p-type $TlInSe_3$ is all higher than that of n-type due to the smoother

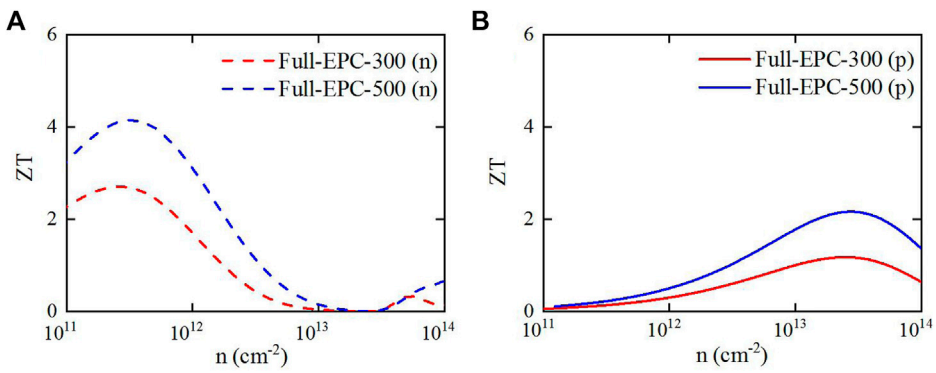

FIGURE 7
(A,B) The ZT values of novel 2D $TlInSe_3$ at 300, and 500 K, respectively.

VBM relative to CBM, resulting in a larger effective carrier mass. Moreover, according to the band convergence strategy, the band degeneracy can further enhance S ($S \propto m^* = N_V^{2/3} m_b^*$). Interestingly, at 300 K, 2D $TlInSe_3$ exhibits a high value of 704 μV/K, compared to TE materials with excellent properties such as PbTe (185 μV/K), Bi_2Te_3 (215 μV/K) and SnSe (~510 μV/K) [45].

Figure 4 displays the calculated results of the electronic thermal conductivity (k_e) and power factor ($S^2\sigma$) at 300 and 500 K, respectively. Since the k_e is dependent on the electrical conductivity, the k_e and σ have similar trends, as exhibited in Figures 4A, B. Furthermore, the calculation reveals that compared with p-type doping, n-type doping of 2D $TlInSe_3$ demonstrates higher conductivity, which leads to larger k_e of n-type. The power factor (*PF*) can be calculated *via* $PF = S^2\sigma$. Figures 4C, D shows the fluctuation of *PF* values of the p-type and n-type doping with the increase of the carrier concentration. Compared with p-type doping, the better conductivity and higher Seebeck coefficient of n-type doping lead to higher PF values. At 300 and 500 K, the maximum values of *PF* are 0.81/0.605 (10^{-2} W/mK^2) for n-type and 0.27/0.23 (10^{-2} W/mK^2) for p-type, respectively. Such a *PF* value is superior to conventional thermoelectric materials such as Bi_2Te_3 [48]and PbTe [49].

Phonons are considered chief carriers for heat transportation in semiconductors and insulators. Here, the k_l can be obtained by summing the contributions of all phonon modes λ and the wave vector q:

$$k_{\alpha\beta} = \frac{1}{V} \sum_{\lambda,q} C_{\lambda,q} \left(v_{\lambda,q}^{\alpha}\right)^2 \tau_{\lambda,q}^{\alpha}, \tag{2a}$$

where V stands for the primitive cell volume, $C_{\lambda,q}$ the specific heat capacity, $v_{\lambda,q}^{\alpha}$ the phonon group velocity, and $\tau_{\lambda,q}^{\alpha}$ the relaxation time. By summing up the radius of Se atoms on the outermost surface together with the van der Waals radius [50, 51], the effective thickness (h) is obtained as 11.2 Å. By employing the iterative method (ITA) and single-mode relaxation time approximation (RTA), and working out the Boltzmann transport equation, the k_l of 2D $TlInSe_3$ was calculated and displayed in Figure 5A. Apparently, at room temperature, the k_l value obtained by the RTA method is 0.25 W/mK, which is much lower than the k_l value (0.46 W/mK) obtained by the ITA method, because the RTA method is more suitable for relatively large samples or slow heating experiment conditions. Moreover, Umklapp scattering controls the heat transport of novel 2D $TlInSe_3$, because the k_l can be fitted well as the function $k_l \propto 1/T$ (the black dashed curve in Figure 5A). Meanwhile, Figure 5B shows that k_l is dominated by phonon and optical branches at a frequency below 3 THz, which indicates that acoustic and low-frequency optical modes contribute significantly to k_l. In addition, a large peak suddenly appears in the frequency range from 5 to 6 THz, indicating that the contribution of the high-frequency optical branch cannot be ignored.

According to Eq. 5, it can be known that the phonon group velocity ($v_{\lambda,q}^2$) and the phonon relaxation time ($\tau_{\lambda,q}$) are the key factors in determining k_l, and these main factors are shown in Figure 6. In Figure 6A, the acoustic phonons in the low-frequency range (frequency <2 THz) are usually considered as the main contributors to the lattice thermal conductivity because of the lager phonon group velocity of the LA mode and ZA mode. Meanwhile, Figure 6A also reveals that the Low-Opt branch possesses a non-negligible phonon group velocity, which indicates that its contribution to the lattice thermal conductivity cannot be ignored. Furthermore, In the frequency range from 5 to 6 THz, the phonon group velocity of the high-frequency optical branch is higher than that of the high-frequency optical branch in other frequency ranges, causing its contribution to the rise of k_l, which is in agreement with the data in Figure 5B. However, for the acoustic branch and the low-frequency optical branch, the phonon group velocity differs little in the low-frequency range (frequency <2 THz), and the main advantage of the acoustic branch comes from $\tau_{\lambda,q}$, as shown in Figure 6B. Figure 6B shows the $\tau_{\lambda,q}$ as a function of frequency. Compared to the optical branch, the acoustic mode clearly dominates. It is worth noting that the rapidly decreasing $\tau_{\lambda,q}$ of the Low-Opt and acoustic branch is beneficial to further reduce the k_l. The total contributions of acoustic modes (ZA, TA, and LA), the Low-Opt branch, and the High-Opt branch to the k_l at different temperatures are shown in Figure 6C. Notably, each phonon mode changes very little, particularly after 300 K, which can be considered as being independent of temperature. The results show that the contribution ratio does not change with temperature after 300 K due to the small change in heat capacity and phonon lifetime with

the increase of temperature. The proportion of the total contribution of acoustic modes to the k_l is about 45% at 300 K, compared to 32% for Low-Opt phonons. Moreover, we also analyze the Güneisen (γ) parameter because it can provide important information about heat transport, which enables the measurement of the anharmonicity of phonons. Figure 6D shows the relationship between the frequency and the γ parameter, with γ ranging from −55 to 10. Such a large value of γ (maximum γ (absolute value) of 55) reflects the strong anharmonicity of phonons, indicating the existence of strong phonon-phonon scattering. Significantly, in the low-frequency range, the acoustic and optical phonons are mixed, dedicating strong acoustic-optic scattering which is consistent with Figure 1B. Based on the above analysis, the strong phonon anharmonicity, especially the ZA and TA modes, as well as the strong acoustic-optic scattering, lead to ultra-low intrinsic lattice thermal conductivity [52, 53].

According to the phonon and electron transport properties, the thermoelectric conversion efficiency (*ZT*) of the new 2D $TlInSe_3$ is obtained, as plotted in Figure 7. In Figure 7A, n-type $TlInSe_3$ has an outstanding ZT value of up to 4.15 at 500 K. The *ZT* values of $TlInSe_3$ are more advantageous than the related materials reported from the literature, such as In_2Se_3 (2.8), TlSe (1.94), and $TlInTe_2$ (2.6). Compared with the ZT of p-type $TlInSe_3$ at 500 K (2.16), the ZT of n-type $TlInSe_3$ at 300 K is more promising. Such high thermoelectric conversion efficiency benefits from ultra-low k_l and outstanding *PF*. Meanwhile, this research demonstrated the novel 2D $TlInSe_3$ as a promising n-type TE material, further expanding the family of TE materials.

4 Conclusion

Overall, we investigate the TE performance of novel two-dimensional $TlInSe_3$ by the first-principles method. By working out the BTE (Boltzmann transport equation), the study reveals that the 2D $TlInSe_3$ possesses an ultra-low k_l of 0.46 W/mK at 300 K, and the analysis of the energy bands suggests that the high Seebeck coefficient is derived from the smooth energy band and band degeneracy. In addition, the performance of the phonon group velocity, phonon anharmonicity, and scattering channel shows that the ultra-low k_l of the novel 2D $TlInSe_3$ is attributed to the stronger phonon anharmonicity, lower phonon group velocity, and the scattering interaction of ZA + O→O, TA + O→O, and LA + O→O process. In addition, the weak Tl-Se chemical bond is also one of the reasons for the low phonon group velocity. Based on studies of electron and phonon transport properties, the ZT values of 2D TlInSe3 are as high as 4.15 at 500 K for n-type and 2.16 for p-type, which suggests that 2D TlInSe3 is a promising thermoelectric material.

Data availability statement

The original contributions presented in the study are included in the article/Supplementary Material, further inquiries can be directed to the corresponding author.

Author contributions

XY: calculation, writing—original draft, visualization. LZ: calculation, writing—original draft, visualization. QW: formal analysis, suggestion, visualization. YL: suggestion, visualization. BL: writing—review and editing, suggestion, software, visualization. All authors contributed to the article and approved the submitted version.

Funding

This work is supported by the Guizhou Provincial Science and Technology Foundation [Grant no. (2019) 1225].

Conflict of interest

The authors declare that the research was conducted in the absence of any commercial or financial relationships that could be construed as a potential conflict of interest.

Publisher's note

Supplementary material

The Supplementary Material for this article can be found online at: https://www.frontiersin.org/articles/10.3389/fphy.2023.1172989/full#supplementary-material

References

1. Gao Z, Wang J-S. Thermoelectric penta-silicene with a high room-temperature figure of merit. *ACS Appl Mater.Interfaces* (2020) 12:14298–307. doi:10.1021/acsami.9b21076

2. Pei Y, Wang H, Snyder GJ. Band engineering of thermoelectric materials. *Adv Mater* (2012) 24:6125–35. doi:10.1002/adma.201202919

3. Kim J, Shim W, Lee W Bismuth nanowire thermoelectrics. *J Mater Chem C* (2015) 3(46), 11999–2013. doi:10.1039/c5tc02886h

4. Pei Y, Shi X, LaLonde A, Wang H, Chen L, Snyder GJ. Convergence of electronic bands for high performance bulk thermoelectrics. *Nature* (2011) 66-69:66–9. doi:10.1038/nature09996

5. Gao Z, Tao F, Ren J Unusually low thermal conductivity of atomically thin 2D tellurium. *Nanoscale* (2018) 10, 12997–3003. doi:10.1039/c8nr01649f

6. Madsen GK, Singh DJ. BoltzTraP. A code for calculating band-structure dependent quantities. *Comput Phys Commun* (2006) 175:67–71. doi:10.1016/j.cpc.2006.03.007

7. Ding G, He J, Cheng Z, Wang X, Li S. Low lattice thermal conductivity and promising thermoelectric figure of merit of zintl type $TlInTe_2$. *J Mater Chem C* (2018) 6: 13269–74. doi:10.1039/c8tc03492c

8. Matsumoto H, Kurosaki K, Muta H, Yamanaka S. Systematic investigation of the thermoelectric properties of $TlMTe_2$ (M= Ga, in, or Tl). *J Appl Phys* (2008) 104:073705. doi:10.1063/1.2987471

9. Jana MK, Pal K, Warankar A, Mandal P, Waghmare UV, Biswas K. Intrinsic rattler-induced low thermal conductivity in zintl type $TlInTe_2$. *J Am Chem Soc* (2017) 139: 4350–3. doi:10.1021/jacs.7b01434

10. Dutta M, Matteppanavar S, Prasad MV, Pandey J, Warankar A, Mandal P, Soni A, Waghmare UV, Biswas K. Ultralow thermal conductivity in chain-like TlSe due to inherent Tl+ rattling. *J Am Chem Soc* (2019) 141:20293–9. doi:10.1021/jacs.9b10551

11. Qiu B, Ruan X. Thermal conductivity prediction and analysis of few-quintuple Bi_2Te_3 thin films: A molecular dynamics study. *Appl Phys Lett* (2010) 97:183107. doi:10.1063/1.3514252

12. Kurosaki K, Yamanaka S. Low-thermal-conductivity group 13 chalcogenides as high-efficiency thermoelectric materials. *Wiley Online Libr* (2013) 210:82–8. doi:10.1002/pssa.201228680

13. Guo Q, Chan M, Kuropatwa B, Kleinke H. Enhanced thermoelectric properties of variants of Tl_9SbTe_6 and Tl_9BiTe_6. *Chem Mater* (2013) 25:4097–104. doi:10.1021/cm402593f

14. Sankar CR, Bangarigadu-Sanasy S, Assoud A, Kleinke H. Syntheses, crystal structures and thermoelectric properties of two new thallium tellurides: Tl_4ZrTe_4 and Tl_4HfTe_4. *J Mater Chem* (2010) 20:7485–90. doi:10.1039/c0jm01363c

15. Patel A, Singh D, Sonvane Y, Thakor P, Ahuja R. High thermoelectric performance in two-dimensional janus monolayer material WS-X (X= Se and Te). *ACS Appl Mater Inter* (2020) 12:46212–9. doi:10.1021/acsami.0c13960

16. Minhas H, Das S, Pathak B. Ultralow thermal conductivity and high thermoelectric performance of γ-GeSe: Effects of dimensionality and thickness. *ACS Appl Energ Mater* (2022) 5:9914–28. doi:10.1021/acsaem.2c01600

17. Ning S, Huang S, Zhang T, Zhang Z, Qi N, Chen Z. Two-dimensional β-PdX_2 (X= S, Se, and Te) monolayers with promising potential for thermoelectric applications. *J Phys Chem C* (2022) 126:17885–93. doi:10.1021/acs.jpcc.2c06186

18. Majumdar A, Chowdhury S, Ahuja R. Drastic reduction of thermal conductivity in hexagonal AX (A= Ga, in and Tl, X= S, Se and Te) monolayers due to alternative atomic configuration. *Nano Energy* (2021) 88:106248. doi:10.1016/j.nanoen.2021.106248

19. Majumdar A, Chowdhury S, Ahuja R. Ultralow thermal conductivity and high thermoelectric figure of merit in two-dimensional thallium selenide. *ACS Appl Energ Mater* (2020) 3:9315–25. doi:10.1021/acsaem.0c01658

20. Nian T, Wang Z, Dong B. Thermoelectric properties of α-in_2Se_3 monolayer. *Appl Phys Lett* (2021) 118(2021):033103. doi:10.1063/5.0036316

21. Zhao L-D, Lo S-H, Zhang Y, Sun H, Tan G, Uher C, Wolverton C, Dravid VP, Kanatzidis MG. Ultralow thermal conductivity and high thermoelectric figure of merit in SnSe crystals. *Nature* (2014) 508:373–7. doi:10.1038/nature13184

22. Sun G, Qin X, Li D, Zhang J, Ren B, Zou T, Xin H, Paschen SB, Yan X. Enhanced thermoelectric performance of n-type Bi_2Se_3 doped with Cu. *J Alloy Compd* (2015) 639: 9–14. doi:10.1016/j.jallcom.2015.03.124

23. Mi W, Qiu P, Zhang T, Lv Y, Shi X, Chen L. Thermoelectric transport of Se-rich Ag_2Se in normal phases and phase transitions. *Appl Phys Lett* (2014) 104:133903. doi:10.1063/1.4870509

24. Wickramaratne D, Zahid F, Lake RK. Electronic and thermoelectric properties of van der Waals materials with ring-shaped valence bands. *J Appl Phys* (2015) 118:075101. doi:10.1063/1.4928559

25. Zheng Y, Tang X, Wang W, Jin L, Li G Large-size ultrathinα-Ga_2S_3 nanosheets toward high-performance photodetection. *Adv Funct Mater* , 2008307,31(2021). doi:10.1002/adfm.202008307

26. Jeengar C, Tomar M, Jindal K, Sharma A, Jha PK. Influence of post deposition annealing on thermoelectric properties of In_2Se_3 thin films. *Mater Sci Semicond Process* (2023) 153(2023):107127. doi:10.1016/j.mssp.2022.107127

27. Li B, Zhang C, Sun Z, Han T, Zhang X, Du J, Wang J, Xiao X, Wang N. The potential thermoelectric material Tl_3XSe_4 (X= V, Ta, Nb): A first-principles study. *Phys Chem Chem Phys* (2022) 24:24447–56. doi:10.1039/d2cp00358a

28. Yang J, Li J, Zhang C, Feng Z, Shi B, Zhai W, Yan Y, Wang Y. Excellent thermoelectric performance of BaMgSi driven by low lattice thermal conductivity: A promising thermoelectric material. *J Alloy Compd* (2020) 827:154342. doi:10.1016/j.jallcom.2020.154342

29. Babich AV, Rogachev M. Investigation of thermal properties and thermal stability of the Sn-Pb-Te system materials for the thermoelectric generator application. Proceeding of the 2020 IEEE Conference of Russian Young Researchers in Electrical and Electronic Engineering (EIConRus). January 2020, St. Petersburg and Moscow, Russia. IEEE (2020). 2111–4.

30. Zhan S, Hong T, Qin B, Zhu Y, Feng X, Su L, Shi H, Liang H, Zhang Q, Gao X, et al. Realizing high-ranged thermoelectric performance in $PbSnS_2$ crystals. *Nat Commun* (2022) 13:5937. doi:10.1038/s41467-022-33684-0

31. Xia Q, Xu Q, Xu B, Yi L. *Ab initio* prediction of thermoelectric performance of monolayer $BiSbTe_3$. *J Solid State Chem* (2021) 296:121963. doi:10.1016/j.jssc.2021.121963

32. Gangwar VK, Kumar S, Singh M, Ghosh L, Yufeng Z, Shahi P, Patil S, Schwier EF, Shimada K, Uwatoko Y. *Pressure induced superconductivity and location of Fermi energy at Dirac point in $BiSbTe_3$* (2019). *arXiv preprint arXiv*:1906.10336.

33. Giannozzi P, Andreussi O, Brumme T, Bunau O, Nardelli MB, Calandra M, Car R, Cavazzoni C, Ceresoli D, Cococcioni M, et al. Advanced capabilities for materials modelling with quantum ESPRESSO. *J Phys Condens Matter* (2017) 29:465901. doi:10.1088/1361-648X/aa8f79

34. Perdew JP, Zunger A. Self-interaction correction to density-functional approximations for many-electron systems. *Phys Rev B* (1981) 23:5048–79. doi:10.1103/physrevb.23.5048

35. Baroni S, Gironcoli SD, Corso AD, Giannozzi P. Phonons and related crystal properties from density-functional perturbation theory. *Rev Mod Phys* (2001) 73: 515–62. doi:10.1103/revmodphys.73.515

36. Gonze X. First-principles responses of solids to atomic displacements and homogeneous electric fields: Implementation of a conjugate-gradient algorithm. *Phys Rev B* (1997) 55:10337–54. doi:10.1103/physrevb.55.10337

37. Li W, Carrete J, Katcho NA, Mingo N. ShengBTE: A solver of the Boltzmann transport equation for phonons. *Comput Phys Commun* (2014) 185:1747–58. doi:10.1016/j.cpc.2014.02.015

38. Lu I-T, Zhou J-J, Park J, Bernardi M. First-principles ionized-impurity scattering and charge transport in doped materials. *Phys Rev Mater* (2022) 6:L010801. doi:10.1103/PhysRevMaterials.6.L010801

39. Peng P-P, Wang C, Li L-W, Li S-Y, Chen Y-Q. Research status and performance optimization of medium-temperature thermoelectric material SnTe. *Chin Phys B* (2022) 31(2022):047307. doi:10.1088/1674-1056/ac20c9

40. Gupta R, Dongre B, Carrete J, Bera C. Thermoelectric properties of the SnS monolayer: Fully *ab initio* and accelerated calculations. *J Appl Phys* (2021) 130:054301. doi:10.1063/5.0058125

41. Zhou J-J, Park J, Lu I-T, Maliyov I, Tong X, Bernardi M. Perturbo: A software package for *ab initio* electron–phonon interactions, charge transport and ultrafast dynamics. *Comput Phys Commun* (2021) 264:107970. doi:10.1016/j.cpc.2021.107970

42. Hieu NN, Phuc HV, Kartamyshev A, Vu TV. Structural, electronic, and transport properties of quintuple atomic janus monolayers Ga_2SX_2 (X= O, S, Se, Te): First-principles predictions. *Phys Rev B* (2022) 105:075402. doi:10.1103/physrevb.105.075402

43. Zhang G, Lu K, Wang Y, Wang H, Chen Q. Mechanical and electronic properties of α– M_2X_3 (M= Ga, in; X= S, Se) monolayers. *Phys Rev B* (2022) 105:235303. doi:10.1103/PhysRevB.105.235303

44. Chen Y, Wu Y, Hou B, Cao J, Shao H, Zhang Y, Mei H, Ma C, Fang Z, Zhu H, et al. Renormalized thermoelectric figure of merit in a band-convergent Sb_2Te_2Se monolayer: Full electron–phonon interactions and selection rules. *J Mater Chem A* (2021) 9: 16108–18. doi:10.1039/d1ta02107a

45. Marfoua B, Hong J. High thermoelectric performance in hexagonal 2D $PdTe_2$ monolayer at room temperature. *ACS Appl Mater.Interfaces* (2019) 11:38819–27. doi:10.1021/acsami.9b14277

46. Cheng L, Liu H, Zhang J, Wei J, Liang J, Shi J, Tang X. Effects of van der Waals interactions and quasiparticle corrections on the electronic and transport properties of Bi_2Te_3. *Phys Rev B* (2014) 90:085118. doi:10.1103/physrevb.90.085118

47. Sheng C, Fan D, Liu H. High thermoelectric performance can be achieved in two-dimensional $(PbTe)_2$ layer. *Phys Lett A* (2020) 384:126044. doi:10.1016/j.physleta.2019.126044

48. Batsanov SS. Van der Waals radii of elements. *Inorg Mater* (2001) 37:871–85. doi:10.1023/A:1011625728803

49. Gao Z, Dong X, Li N, Ren J. Novel two-dimensional silicon dioxide with in-plane negative Poisson's ratio. *Nano Lett* (2017) 17:772–7. doi:10.1021/acs.nanolett.6b03921

50. Yuan K, Sun Z, Zhang X, Gong X, Tang D A first-principles study of the thermoelectric properties of rhombohedral GeSe. *Phys Chem Chem Phys* 22, 1911, 22. doi:10.1039/c9cp05153h2020).

51. Lv B, Hu X, Wang N, Song J, Liu X, Gao Z Thermal transport property of novel two-dimensional nitride phosphorus: An *ab initio* study. *Appl Surf Sci* (2021) 559, 149463. doi:10.1016/j.apsusc.2021.149463

52. Peng B, Zhang H, Shao H, Xu Y, Zhang X, Zhu H Low lattice thermal conductivity of stanene. *Sci Rep* ,6, 20225, doi:10.1038/srep202252016).

53. Wang Y, Gao Z, Zhou J Ultralow lattice thermal conductivity and electronic properties of monolayer 1T phase semimetal $SiTe_2$ and $SnTe_2$. *Phys E* (2019) 108, 53–9. doi:10.1016/j.physe.2018.12.004